Direct measurement of electron affinity of carbazole-based self-assembled monolayer used as hole-selective layer in high-efficiency perovskite solar cells

Aruto Akatsuka[1)], Makoto Miura[1)], Gaurav Kapil[2)], Shuzi Hayase[2,3)] and Hiroyuki Yoshida[4,5)*]

1) Graduate School of Science and Engineering, Chiba University, 1-33 Yayoi-cho, Inage-ku, Chiba, 263-8522, Japan.
2) i-Powered Energy System Research Center, The University of Electro-Communications, 1-5-1 Chofugaoka, Chofu, Tokyo, 182-8585, Japan.
3) Graduate School of Informatics and Engineering, The University of Electro-Communications, 1-5-1 Chofugaoka, Chofu, Tokyo, 182-8585, Japan.
4) Graduate School of Engineering, Chiba University, 1-33 Yayoi-cho, Inage-ku, Chiba, 263-8522, Japan.
5) Molecular Chirality Research Center, Chiba University, 1-33 Yayoi-cho, Inage-ku, Chiba, 263-8522, Japan.

Abstract

Carbazole-based self-assembled monolayers (SAMs) have received considerable attention as hole-selective layers (HSLs) in inverted perovskite solar cells. As an HSL, the electron-blocking capability is important and directly related to electron affinity (EA). Low-energy inverse photoelectron spectroscopy (LEIPS) is the most reliable method for EA measurement. However, the intense electron-impact-induced fluorescence from the carbazole interferes with the measurement. By improving the photon detector, we were able to measure 2PACz and MeO-2PACz LEIPS spectra and determine their respective EAs of 1.73 eV and 1.48 eV. These small EA values ensure effective electron-blocking capability of HSLs regardless of the type of perovskite layer.

*Corresponding Author: hyoshida@chiba-u.jp

Perovskite solar cells (PSCs) have attracted tremendous attention because they can be fabricated by a low-cost solution process and achieve a power conversion efficiency (PCE) of 26.1% [1]. 2,2',7,7'-Tetrakis[N,N-di(4-methoxyphenyl)amino]-9,9'-spirobifluorene (spiro-OMeTAD) is exclusively used as a hole-selective layer (HSL) in a normal (n-i-p) structure PSC with high PCE. However, spiro-OMeTAD requires doping and has stability issues [2]. On the other hand, such stable polymers as poly(3,4-ethylenedioxythiophene)/poly(4-styrenesulfonate) (PEDOT:PSS) and poly[bis(4-phenyl)(2,4,6-trimethylphenyl)amine] (PTAA) are used as an HSL in an inverted (p-i-n) structure PSC [3]. However, the polymer layer is usually around 10 to 40 nm thick, which decreases light transmission and electrical conductivity [4].

A self-assembled monolayer (SAM) has been developed as a substitute for these polymer HSLs. As SAM-based HSL is very thin (approximately 1 nm) [5] and firmly binds to a transparent electrode, it hardly absorbs light and has high stability [4]. Among the various SAM materials, carbazole derivatives are the most widely studied. A carbazole-based SAM molecule comprises a carbazole backbone, an anchor moiety binding to the transparent electrode surface, and an alkyl chain connecting the carbazole backbone and the anchor moiety. The SAM molecules with alkyl chains C_nH_{2n} of various lengths (n = 2, 4, 6) and substituents such as methyl and methoxy groups have been developed [6].

To achieve good performance as HSL, high hole collection efficiency and electron-blocking capability are required, and these can be assessed from the HOMO and LUMO energy levels, respectively. If the vacuum level alignment is assumed for simplicity, the ionization energy (IE; HOMO energy level with reference to the vacuum level) should lie between the IE of the perovskite surface and the work function of the transparent electrode. Conversely, the electron affinity (EA; the LUMO energy level with reference to the vacuum level) should be smaller than that of the perovskite layer for electron blocking. Therefore, precise and reliable IE and EA values of HSL are essential to evaluate and choose a suitable SAM material. In addition, interfacial hole/electron recombination crucially impacts PSC performance. The recombination rate depends on IE and EA as well as the trap density [6,7]. To discuss the recombination dynamics in detail, accurate IE and EA values of HSL are indispensable.

IE in a solid can be determined by ultraviolet photoelectron spectroscopy (UPS) measurement of a film. Conversely, EA is often predicted from the IE and the optical gap [4] assuming that the transport gap (IE–EA) is equal to the optical gap. However, the transport gap and the optical gap differ owing to the exciton binding energy (usually ranging from 0.2 eV to 1 eV) for organic

materials [8-10]. Thus, EA is often overestimated from the IE and the optical gap. IE and EA are also estimated from the oxidation and reduction potentials derived from cyclic voltammetry (CV) measurement. However, CV data are affected by the solvent and the supporting electrolyte, and the measured values differ from those in the film [11-14]. In principle, EA can be best measured by inverse photoelectron spectroscopy (IPES), which is regarded as the inversion process of UPS. However, damage to organic materials by electron irradiation has hindered the application of conventional IPES. Although IPES has provided unprecedent information about the unoccupied states of organic semiconductors over 30 years [15-20], its applicability is limited. The development of low-energy IPES (LEIPS) has made precise EA measurement possible [21,22]. In LEIPS, an electron with less than 5 eV kinetic energy (i.e., the damage threshold of most organic materials) and a photon emitted by the radiative transition from a free electron to the unoccupied states (including LUMO) are detected. As the photon energy is in the near-ultraviolet or visible range, the photons are detected by a combination of a bandpass filter and a photomultiplier. LEIPS has enabled thickness-dependent measurements to study the interface energy level alignment of unoccupied states [23], the precise determination of exciton binding energy [8] and polarization energy [24-26], the electron injection barrier in organic light emitting diode [27], analysis of the charge separation mechanism in organic solar cells [28,29] and measuring the on-site coulomb repulsion energy (Hubberd U) in polymers [30], etc. Recently, the angle-resolved measurement to observe conduction band structure [31,32] has been achieved, which has never been possible with the conventional IPES. However, the application of LEIPS to fluorescent molecules such as carbazole derivatives is not straightforward because the carbazole derivatives generate intense electron-induced fluorescence that interferes with the detection of the weak photon signal by LEIPS. To observe the LEIPS spectrum of the carbazole derivatives, we need to improve the experimental setup.

In this paper, we report EA measurements of carbazole-based SAMs as HSL using LEIPS. We choose the two most widely used materials (2-(9H-Carbazol-9-yl)ethyl)phosphonic acid (2PACz) and (2-(3,6-Dimethoxy-9H-carbazol-9-yl)ethyl)phosphonic acid (MeO-2PACz) as examples. First, we explain the problem arising from the EA measurement of the SAMs using LEIPS. Second, we show an improved experimental setup to solve this problem. Third, we measure the LEIPS spectra of 2PACz and MeO-2PACz. The determined EAs corroborate the good electron-blocking capability of these SAMs as HSL.

2PACz and MeO-2PACz film samples were prepared by spin coating 1 mM solutions of 2PACz and MeO-2PACz in isopropyl alcohol (IPA) onto ITO substrates at the University of Electro-

Communications. After annealing the samples at 100 ℃ for 10 minutes, the unbonded 2PACz and MeO-2PACz molecules on the ITO substrates were washed off with IPA, and the washed samples were annealed at 100 ℃ for 1 min to remove the solvent.

The samples were kept in a nitrogen atmosphere and transported to Chiba University for LEIPS measurement. The details of the LEIPS setup are described elsewhere [33]. The samples were irradiated with 1.0 to 6.5 eV electron beams. The emitted photons were detected by a bandpass detector consisting of a bandpass filter and a photomultiplier. We have used the photomultiplier tube, Hamamatsu Photonics R585s, since the development of LEIPS because of its low dark counts. We find that the photomultiplier tube should be replaced in this work. Because the photon detector is key to this work, we will discuss the details later. The work function was measured from the onset of the sample current as a function of electron kinetic energy.

Figure 1 shows the LEIPS spectra of 2PACz measured with a bandpass filter (center wavelengths of 232 nm and 260 nm) and a photomultiplier tube (Hamamatsu Photonics R585s). The spectral onset shifted from -0.22 eV to 0.42 eV when the bandpass filter was changed from 232 nm to 260 nm. If the photon signal originated from the IPES process, the electron binding energy $E_b = h\nu - E_k$ should be independent of the photon energy $h\nu$. Because the onset difference of 0.6 eV corresponds approximately to the photon energy difference, 5.3 eV (232 nm) and 4.8 eV (260 nm), the process depends only on the electron energy E_k. Furthermore, the signal was observed even below the Fermi level when the photon with the wavelength of 232 nm was detected. Likely, the photon signal did not originate from the IPES process.

It is known that molecules display fluorescence by electron-impact excitation and photon excitation [34]. Carbazole is a highly emissive molecule that shows fluorescence by electron impact [35]. Its spectrum is similar to photon-excited fluorescence due to the S1->S0 transition from 330 nm to 400 nm. It was reported that a small amount of impurities in carbazole samples may cause fluorescence [36]. We used a bandpass filter with a center wavelength of 232 nm (5.28 eV) or 260 nm (4.79 eV), the energy of which seemed too high for fluorescence detection below 330 nm, and inspected the sensitivity curves of our photon detector. Figure 2 shows the quantum efficiencies of the R585s photomultiplier tube and of the photon detector combined with the bandpass filters. The photon detector shows high sensitivity at the center wavelength of the bandpass filter (260 or 232 nm) and the long tail extending toward the long-wavelength region. Even around 330–400 nm where carbazole shows strong fluorescence, the photon detector has low but non-negligible sensitivity. Because the photon signal intensity is the sensitivity integrated over the wavelength,

the signal intensity of the photon detector tail region should be sufficiently high. Furthermore, the inverse photoelectron process has a very small cross section [37], and typical photon intensity in the present measurement ranges from 10 to 100 cps, whereas the fluorescence induced by the electron impact is so intense that it is sometimes visible to the naked eye. Therefore, we conclude that the fluorescence from carbazole is so strong that a sufficient amount of photons are transmitted through the bandpass filter to be detected by the photomultiplier tube.

The R585s photomultiplier tube uses a bi-alkali (Sb-Rb-Cs and Sb-K-Cs) photocathode and has a sensitivity range of 700 nm to 160 nm (Figure 2). Conversely, a photomultiplier tube with a Cs-Te "solar-blind" photocathode is not sensitive to wavelengths longer than 300 nm [38]. Aiming to avoid the intense photon signal in the visible range, we combined a Cs-Te photomultiplier tube with near-ultraviolet bandpass filters. Unfortunately, the Cs-Te photomultiplier tube for photon counting use is not available, so we specially selected a low dark count tube from the manufacture's stock of Hamamatsu Photonics R821 and used it for photon counting.

Note that this problem is specific to LEIPS, because LEIPS analyzes visible/near-UV photons whose energies are close to those of molecular fluorescence in the visible range. The high energy selectivity is crucial to safely observe the LEIPS signal. Conversely, the conventional IPES using the bandpass photon detector in the vacuum ultraviolet range has a sufficient energy difference to block the molecular fluorescence. The photon detector developed by Dose, using a gas-filled Geiger-Mueller counter [39] is totally insensitive to photons below the ionization energy of the filled gas (> 9 eV of I_2, isopropanol, acetone, etc. [40]). The solid-state bandpass detector using the CuBe electron multiplier [41], which was later improved by coating the first dynode with an alkali halide [42], also has negligible sensitivity in the visible range.

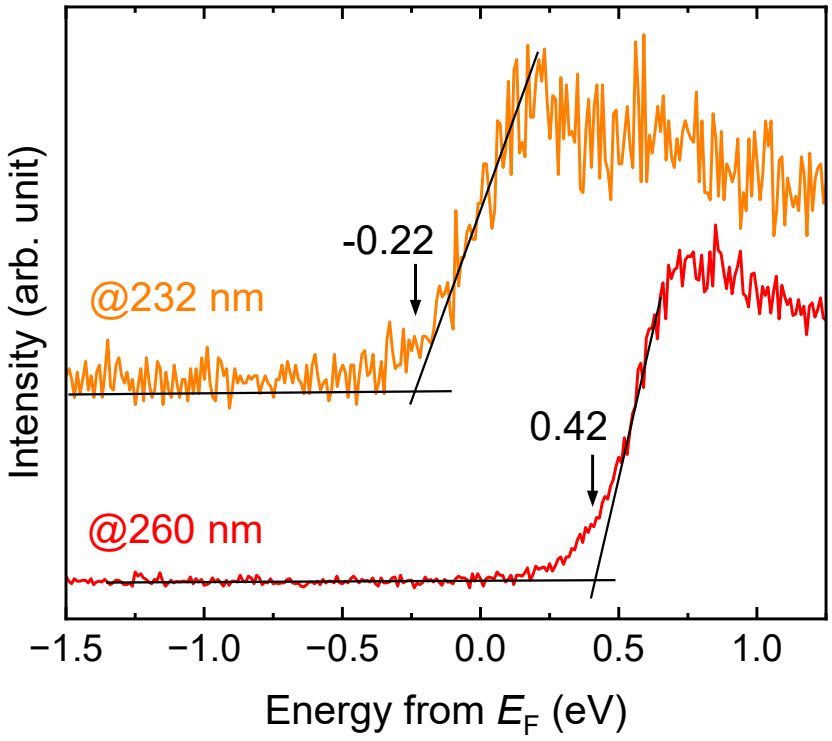

Figure 1: LEIPS spectra of 2PACz measured with a bandpass filter (232 and 260 nm) and a photomultiplier tube (Hamamatsu Photonics R585s).

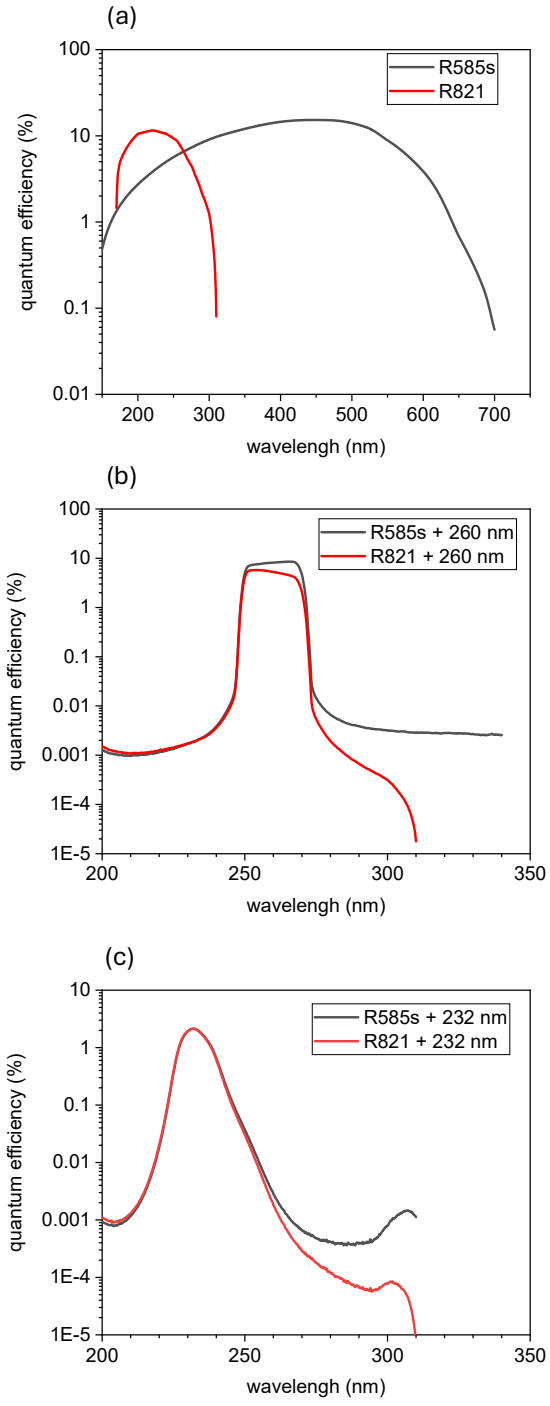

Figure 2: Sensitivity curves of photon detector. (a) Quantum efficiencies of photomultiplier tubes R585s [43] and R821[44]. (b) Comparison of quantum efficiencies of photon detector comprised of the bandpass filter (260 nm) and photomultiplier tubes R585s and R821. (c) The same as panel (b) except for the bandpass filter with a center wavelength of 232 nm.

Figure 3 shows the LEIPS spectra of 2PACz and MeO-2PACz measured with the photon detector consisting of a bandpass filter with a center wavelength of 285 nm and the photomultiplier tube R821. We observed clear onsets at 3.49 eV (2PACz) and 3.32 eV (MeO-2PACz) above the Fermi level. The LEIPS spectrum of pristine ITO substrate exhibits a gradual rise around 1 eV (not shown). We assigned the small increases in the background to the signal from the ITO substrate. When the 285 nm bandpass filter was replaced with a 260 nm one, the onset energies in the E_k scale shifted by 0.51 eV, but the electron binding energies E_b were unchanged (3.42 eV for 2PACz and 3.19 eV for MeO-2PACz), confirming that the spectral onsets originated from the IPES process, namely, the transition from a free electron to the LUMO energy levels. The LEET spectra in Figure 3 show that the work functions (or the vacuum level) are 5.21 eV (2PACz) and 4.80 eV (MeO-2PACz). Using these work functions, we determined EAs to be 1.73 eV (2PACz) and 1.48 eV (MeO-2PACz) as the difference between the LEIPS onset and the vacuum level (Figure 4).

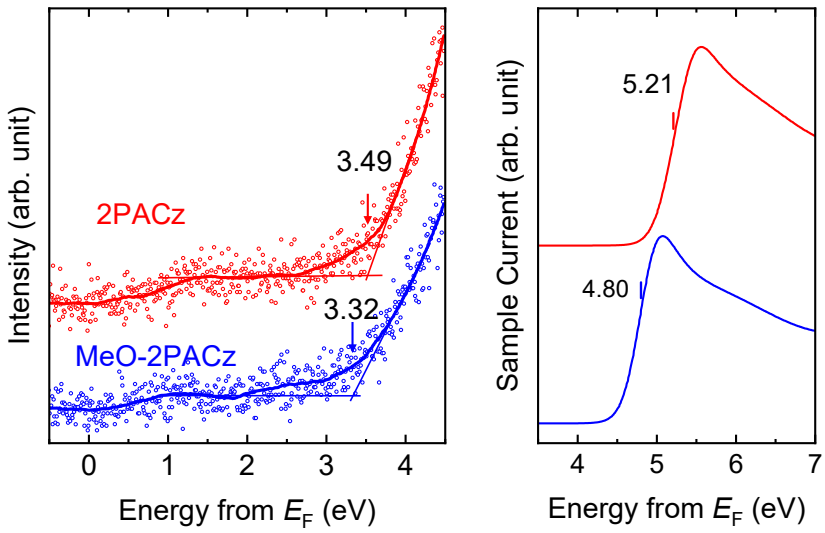

Figure 3: LEIPS (left) and LEET (right) spectra of 2PACz and MeO-2PACz measured by the improved photon detector using the photomultiplier tube R821 and the bandpass filter with a center wavelength of 285 nm.

The reported IEs are 5.6 eV [45]-5.9 eV [46] for 2PACz and 5.1 eV [45] for MeO-2PACz. The optical gaps are 3.5 eV (2PACz) and 3.2 eV (MeO-2PACz) [45,46]. These values and the EAs determined in this work are summarized in Figure 4. The transport gaps calculated as the difference between

IE and EA are 4.0–4.3 eV for 2PACz and 3.6 eV for MeO-2PACz. In previous studies, the EA (or LUMO energy level) was estimated from the IE and the optical gap [45-49]. The estimated EA are systematically about 0.5 eV larger (or the LUMO level is lower) than the LEIPS measurements. The transmission coefficient for electron tunneling or the carrier population at the barrier is exponentially related to the energy difference [50]. If we take the energy levels shown in Fig. 4, the SAM thickness of 1 nm, the difference of 0.5 eV in barrier height leads to a four orders of magnitude difference in the transmission coefficient for electron tunneling. The electron density in the LUMO of the SAM layer can be up to 10 orders of magnitude different, assuming the Boltzmann distribution (the values vary slightly depending on the energy parameters, but do not affect the main conclusion). These estimates show that a difference of only 0.5 eV in barrier height can make a significant difference in electron blocking capability, highlighting the importance of accurate measurement of EA values.

We calculated the exciton binding energies from the difference between the transport and optical gaps, and they were 0.5–0.8 eV for 2PACz and 0.4 eV for MeO-2PACz. We recently reported that the exciton binding energy of organic semiconductors and polymers is approximately 1/4 of the transport gap and 1/3 of the optical gap [8]. Although we predicted an exciton binding energy of approximately 1 eV, the observed exciton binding energies are smaller than this prediction probably because a positive or negative charge is stabilized near the metallic electrodes owing to the efficient screening [23].

From the obtained EAs, we discuss the electron-blocking capability of SAMs. The energy level alignment at the SAM–perovskite interface should lie between two limiting cases, namely, the Fermi level alignment (the Schottky limit) and the vacuum level alignment (the Bardeen limit). Figure 4 shows the conduction band (CB) minima and the valence band (VB) maxima with the Fermi level alignment of representative perovskite $CH_3NH_3PbI_3$ ($MAPbI_3$) and wide band gap perovskite for silicon/perovskite tandem solar cell $Cs_{0.2}NH_2CH{=}NH_2(FA)_{0.8}PbI_3Br_{1.2}$ ($Cs_{0.2}FA_{0.8}PbI_{1.8}Br_{1.2}$). The UPS and LEIPS of $MAPbI_3$ measured at normal angles cannot access the VB and CB edges (VB at -1.55 eV and CB at 0.97 eV from the Fermi level, respectively [51]) owing to band dispersion [52,53]. We show the corrected energy levels of $MAPbI_3$ in Figure 4 [51]. The LUMO energy levels of the SAMs are located more than 3 eV above the CB of the both perovskite layers in the case of the Schottky limit. On the other hand, assuming a vacuum level alignment, the energy barrier (difference between the LUMO energy level of SAM and the CB of perovskite) becomes approximately 2 eV, which is still sufficiently high to efficiently block the electrons at the SAM/perovskite also in the Bardeen limit. Because the band gaps of perovskites

for efficient PSCs are between 1 and 2 eV (theoretically, the best optical gap is 0.8–1.4 eV for the single cell and 1.7 eV and 1 eV for the double-layered tandem cell [56]), the LUMO energy level of the present SAMs is expected to always be well above the CB of any perovskite layer for the PSC.

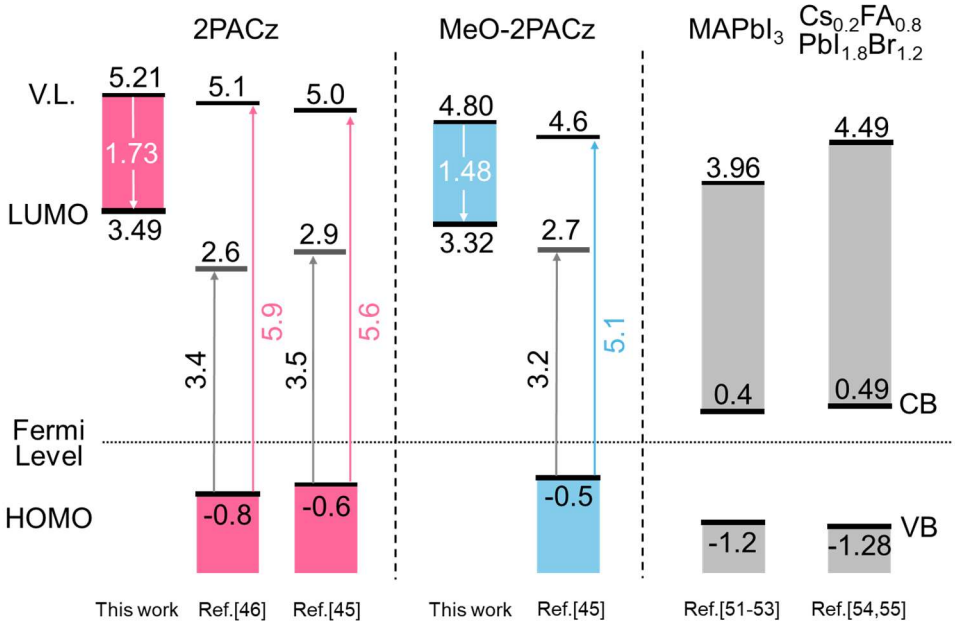

Figure 4: Energy level diagram of carbazole-based SAMs 2PACz and MeO-2PACz, and perovskites $MAPbI_3$ [51-53] and $Cs_{0.2}FA_{0.8}PbI_{1.8}Br_{1.2}$ [54,55]. The values (in eV) are with reference to the Fermi level except for the electron affinities (numbers in white) and the optical transition energies (numbers in black rotated upward by 90°) and the ionization energies (numbers in red/blue rotated upward by 90°).

In conclusion, we established an experimental method to determine the EAs of carbazole derivatives in a solid. The EA values of organic materials are best determined by LEIPS. However, when the sample surface is irradiated with an electron beam for LEIPS measurement, the carbazole derivatives emit strong fluorescence induced by electron impact in the visible range, which interferes with the LEIPS measurement. We used a "solar-blind" photomultiplier tube with a Cs-Te photocathode to separate the LEIPS signal from the fluorescence and observed the LEIPS spectra. The present method applies to not only carbazole-based SAMs but also other emissive organic semiconductors. We applied this technique to prototypical carbazole SAMs used as HSL

and determined their EAs to be 1.73 eV (2PACz) and 1.48 eV (MeO-2PACz). These EAs are smaller than the previously reported values, implying that the carbazole-based SAMs have better electron blocking capability than previously thought.

Acknowledgments

We thank Mr. Daisuke Hamamura for his help in measuring UV-vis spectra and Prof. Kazuki Nakamura of Chiba University for allowing us to use the UV-vis spectrometer. This work was supported by JST−MIRAI (JPMJMI22E2) and JSPS-KAKENHI (23H03939).

Conflict of interest declaration

The authors have no conflicts of interest to disclose.

Data Availability

Supporting data for this study are available from the corresponding author upon reasonable request.

Author Contributions

HY, AA, and SH planned this work. MM and HY developed the photon detector. AA and MM measured and analyzed the data. GK and SH prepared the samples. AA and HY wrote the manuscript.

References

[1] NREL. Best Research-Cell Efficiency Chart, 2024, https://www.nrel.gov/pv/cell-efficiency.html

[2] Zhang, T., Wang, F., Kim, H., Choi, I., Wang, C., Cho, E., Konefal, R., Puttisong, Y., Terado, K., Kobera, L., Chen, M., Yang, M., Bai, S., Yang, B., Suo, J., Yang, S., Liu, X., Fu, F., Yoshida, H., Chen, W. M., Brus, J., Coropceanu, V., Hagfeldt, A., Brédas, J., Fahlman, M., Kim, D., Hu, Z., Gao, F., Ion-modulated radical doping of spiro-OMeTAD for more efficient and stable perovskite solar cells. *Science* **377**, 495-501 (2022). DOI:10.1126/science.abo2757

[3] Yao, Y., Cheng, C., Zhang, C., Hu, H., Wang, K., De Wolf, S., Organic Hole-Transport Layers for Efficient, Stable, and Scalable Inverted Perovskite Solar Cells. *Adv. Mater.* **34**, 2203794 (2022).
DOI: 10.1002/adma.202203794

[4] Wang, S., Guo, H., Wu, Y., Advantages and challenges of self-assembled monolayer as a hole-selective contact for perovskite solar cells. *Mater. Futures* **2**, 012105 (2023).
DOI: 10.1088/2752-5724/acbb5a

[5] Magomedov, A., Al-Ashouri, A., Kasparavičius, E., Strazdaite, S., Niaura, G., Jošt, M., Malinauskas, T., Albrecht, S., Getautis, V., Self-assembled hole transporting monolayer for highly efficient perovskite solar cells, *Adv. Energy Mater.* **8,** 1801892 (2018).
DOI: 10.1002/aenm.201801892

[6] Levine, I., Al-Ashouri, A., Musiienko, A., Hempel, H., Magomedov, A., Drevilkauskaite, A., Getautis, V., Menzel, D., Hinrichs, K., Unold, T., Albrecht, S., Dittrich, T., Charge transfer rates and electron trapping at buried interfaces of perovskite solar cells, *Joule* **11**, 2915-2933 (2021).
DOI: 10.1016/j.joule.2021.07.016

[7] Stolterfoht, M., Caprioglio, P., Wolff, C. M., Márquez, J. A., Nordmann, J., Zhang, S., Rothhardt, D., Hörmann, U., Amir, Y., Redinger, A., Kegelmann, L., Zu, F., Albrecht, S., Koch, N., Kirchartz, T., Saliba, M., Unold, T., Neher, D., The impact of energy alignment and interfacial recombination on the internal and external open-circuit voltage of perovskite solar cells, *Energy Environ. Sci.* **12**, 2778-2788 (2019).
DOI: 10.1039/C9EE02020

[8] Sugie, A., Nakano, K., Tajima, K., Osaka, I., Yoshida, H., Dependence of Exciton Binding Energy on Bandgap of Organic Semiconductors, *J. Phys. Chem. Lett.* **14**, 11412–11420

(2023).
DOI: 10.1021/acs.jpclett.3c02863

[9] Hill, I.G., Kahn, A., Soos, Z.G., Pascal, Jr, R.A., Charge-separation energy in films of π-conjugated organic molecules, *Chem. Phys. Lett.* **327**, 181-188 (2000).
DOI: 10.1016/S0009-2614(00)00882-4

[10] Knupfer, M., Exciton binding energies in organic semiconductors, *Appl. Phys. A* **77**, 623-626 (2003).
DOI: 10.1007/s00339-003-2182-9

[11] Sworakowski, J., How accurate are energies of HOMO and LUMO levels in small-molecule organic semiconductors determined from cyclic voltammetry or optical spectroscopy?, *Synth. Met.* **235**, 125-130 (2018).
DOI: 10.1016/j.synthmet.2017.11.013

[12] Kubo, M., Yoshida, H., Electron affinities of small-molecule organic semiconductors: Comparison among cyclic voltammetry, conventional inverse photoelectron spectroscopy, and low-energy inverse photoelectron spectroscopy, *Org. Electron.* **108**, 106551 (2022).
DOI: 10.1016/j.orgel.2022.106551.

[13] Djurovich, P. I., Mayo, E. I., Forrest, S. R., Thompson, M. E., Measurement of the lowest unoccupied molecular orbital energies of molecular organic semiconductors, *Org. Electron.* **10**, 515-520 (2009).
DOI: 10.1016/j.orgel.2008.12.011

[14] Sworakowski, J., Lipiński, J., Janus, K., On the reliability of determination of energies of HOMO and LUMO levels in organic semiconductors from electrochemical measurements. A simple picture based on the electrostatic model, *Org. Electron.* **33**, 300-310 (2016).
DOI: 10.1016/j.orgel.2016.03.031

[15] Frank, K. H., Yannoulis, P., Dudde, R., Koch, E. E., Unoccupied molecular orbitals of aromatic hydrocarbons adsorbed on Ag(111), *J. Chem. Phys.* **89**, 7569- 7576 (1988).
DOI: 10.1063/1.455720

[16] Hill, I.G., Kahn, A., Cornil, J., dos Santos, D.A., Brédas, J.L., Occupied and unoccupied electronic levels in organic π-conjugated molecules: comparison between experiment and theory, *Chem. Phys. Lett.* **317**, 444-450 (2000).
DOI: 10.1016/S0009-2614(99)01384-6

[17] Yoshida, H., Tsutsumi, K., Sato, N., Unoccupied electronic states of 3d-transition metal phthalocyanines (MPc: M=Mn, Fe, Co, Ni, Cu and Zn) studied by inverse photoemission

spectroscopy, *J. Electron Spectros. Relat. Phenom.* **121**, 83-91 (2001).
DOI: 10.1016/S0368-2048(01)00328-0

[18] Zahn, D. R.T., Gavrila, G. N., Gorgoi, M., The transport gap of organic semiconductors studied using the combination of direct and inverse photoemission, *Chem. Phys*. **325**, 99-112 (2006).
DOI: 10.1016/j.chemphys.2006.02.003

[19] Krause, S., Casu, M. B., Schöll, A., Umbach, E., Determination of transport levels of organic semiconductors by UPS and IPS, *New J. Phys.* **10**, 085001 (2008).
DOI: 10.1088/1367-2630/10/8/085001

[20] Kanai, K., Akaike, K., Koyasu, K., Sakai, K., Nishi, T., Kamizuru, Y., Nishi, T., Ouchi, Y., Seki, K., Determination of electron affinity of electron accepting molecules, *Appl. Phys. A* **95**, 309-313 (2009).
DOI: 10.1007/s00339-008-5021-1

[21] Yoshida, H., Near-ultraviolet inverse photoemission spectroscopy using ultra-low energy electrons, *Chem. Phys. Lett.* **539-540**, 180-185 (2012).
DOI: 10.1016/j.cplett.2012.04.058

[22] Yoshida, H., Principle and application of low energy inverse photoemission spectroscopy: A new method for measuring unoccupied states of organic semiconductors, *J. Electron Spectrosc. Relat. Phenom.* **204**, 116-124, (2015).
DOI: 10.1063/1.4860055

[23] Aihara, T., Abd-rahman, S., Yoshida, H., Metal screening effect on energy levels at metal/organic interface: Precise determination of screening energy using photoelectron and inverse-photoelectron spectroscopies, *Phys. Rev. B* **104**, 085305 (2021).
DOI: 10.1103/PhysRevB.104.085305

[24] Yamada, K., Yanagisawa, S., Koganezawa, T., Mase, K., Sato, N., Yoshida, H., Impact of the molecular quadrupole moment on ionization energy and electron affinity of organic thin films: Experimental determination of electrostatic potential and electronic polarization energies, *Phys. Rev. B* **97**, 245206 (2018).
DOI: 10.1103/PhysRevB.97.245206

[25] Uemura, Y., Abd-Rahman, S. A., Yanagisawa, S., Yoshida, H., Quantitative analysis of the electrostatic and electronic polarization energies in molecularly mixed films of organic semiconductors, *Phys. Rev. B* **102**, 125302 (2020).
DOI: 10.1103/PhysRevB.102.125302

[26] Abd-Rahman, S. A., Yamaguchi, T., Kera, S., Yoshida, H., Sample-shape dependent energy levels in organic semiconductors, *Phys. Rev. B* **106**, 075303 (2022).
DOI: 10.1103/PhysRevB.106.075303

[27] Sasaki, T., Hasegawa, M., Inagaki, K., Ito, H., Suzuki, K., Oono, T., Morii, K., Shimizu, T., Fukagawa, H., Unravelling the electron injection/transport mechanism in organic light-emitting diodes, *Nature Comm.* **12**, 2706 (2021).
DOI: 10.1038/s41467-021-23067-2

[28] Nakano, K., Chen, Y., Xiao, B., Han, W., Huang, J., Yoshida, H., Zhou, E., Tajima, K., Anatomy of the energetic driving force for charge generation in organic solar cells, *Nature Comm.* **10**, 2520 (2019).
DOI: 10.1038/s41467-019-10434-3

[29] Bertrandie, J., Han, J., De Castro, C. S. P. Yengel, E., Gorenflot, J., Anthopoulos, T., Laquai, F., Sharma, A., Baran, D., The Energy Level Conundrum of Organic Semiconductors in Solar Cells, *Adv. Mater.* **34**, 2202575 (2022).
DOI: 10.1002/adma.202202575

[30] Lungwitz, D., Joy, S., Mansour, A. E., Opitz, A., Karunasena, C., Li, H., Panjwani, N. A., -Moudgil, K., Tang, K., Behrends, J., Barlow, S., Marder, S. R., Brédas, J., Graham, K., Koch, N., Kahn, A., Spectral Signatures of a Negative Polaron in a Doped Polymer Semiconductor: Energy Levels and Hubbard U Interactions, *J. Phys. Chem. Lett*. **14**, 5633-5640 (2023).
DOI: 10.1021/acs.jpclett.3c01022

[31] Sato, H., Abd. Rahman, S. A., Yamada, Y., Ishii, H., Yoshida, H., Conduction band structure of high-mobility organic semiconductors and partially dressed polaron formation, *Nature Mat.* **21**, 910-916 (2022).
DOI: 10.1038/s41563-022-01308-z

[32] Yang, J., Sato, H., Orio, H., Liu, X., Fahlman, M., Ueno, N., Yoshida, H., Yamada, T., Kera, S., Accessing the Conduction Band Dispersion in CH3NH3PbI3 Single Crystals, *J. Phys. Chem. Lett.* **12**, 3773-3778 (2021).
DOI: 10.1021/acs.jpclett.1c00530

[33] Yoshida, H., Low energy inverse photoemission spectroscopy apparatus, *Rev. Sci. Instrum.* **85**, 016101 (2014).
DOI: 10.1016/j.cplett.2012.04.058

[34] Kukhta, A. V., Kazakov, S. M., Spectroscopy of the interaction of a low-energy electron

beam with organic luminescent molecules, *Phys.-Usp.* **66**, 173-181 (2023).
DOI: 10.3367/UFNe.2022.05.039197

[35] Borisevich, N. A., Kazakov, S. M., Kolesnik, É. É., Kukhto, A. V., Mit'kovets, A. I., Murtazaliev, D. V., Raichenok, T. F., Khristoforov, O. V., Spectral-Luminescence Characteristics of Carbazole, Dibenzofuran, and Dinaphthofuran in the Gas Phase in Excitation by Electrons and Photons, *J. Appl. Spectrosc.* **68,** 871-876 (2001).
DOI: 10.1023/A:1013262404759

[36] Chen, C., Chi, Z., Chong, K. C. Batsanov, A. S. Yang, Z., Mao, Z., Yang, Z., Liu, B., Carbazole isomers induce ultralong organic phosphorescence, *Nat. Mater.* **20,** 175-180 (2021).
DOI: 10.1038/s41563-020-0797-2

[37] Pendry, J. B., New Probe for Unoccupied Bands at Surfaces, *Phys. Rev. Lett.* **45**, 1356 (1980).
DOI: 10.1103/PhysRevLett.45.1356

[38] Hamamatsu Photonics K.K., Photomultiplier Tubes Basic and Applications, 4th Ed., Hamamatsu Photonics K.K. Electron Tube Division, Japan, 2017, pp. 246.

[39] Dose, V., VUV isochromat spectroscopy, *Appl. phys.* **14**, 117-118 (1977).
DOI: 10.1007/BF00882639

[40] Thiede, C., Niehues, I., Schmidt, A. B., Donath, M., The acetone bandpass detector for inverse photoemission: operation in proportional and Geiger–Müller modes, *Meas. Sci. Technol.* **29**, 065901 (2018).
DOI: 10.1088/1361-6501/aab941

[41] Babbe, N., Drube, W., Schafer, I., Skibowski, M., A simple and compact system for combined angular resolved inverse photoemission and photoemission in the vacuum ultraviolet, *J. Phys. E: Sci. Instrum.* **18**, 158 (1985).
DOI: 10.1088/0022-3735/18/2/014

[42] Schäfer, I., Drube, W., Schlüter, M., Plagemann, G., Skibowski, M., Bandpass photon detector with high efficiency for inverse photoemission spectroscopy, *Rev. Sci. Instrum.* **58**, 710-711 (1987).
DOI: 10.1063/1.1139244

[43] Hamamatsu Photonics K.K., Photomultiplier Tubes R464, R585, 2016, https://www.hamamatsu.com/content/dam/hamamatsu-photonics/sites/documents/99_SALES_LIBRARY/etd/R464_R585_TPMH1140E.pdf

[44] Hamamatsu Photonics K.K., Photomultiplier Tubes R821, 1998, https://www.hamamatsu.com/content/dam/hamamatsu-photonics/sites/documents/99_SALES_LIBRARY/etd/R821_TPMH1210E.pdf

[45] Al-Ashouri, A., Magomedov, Ar., Roß, M., Jošt, M., Talaikis, M., Chistiakova, G., Bertram, T., Márquez, J. A., Köhnen, E., Kasparavičius, E., Levcenco, S., Gil-Escrig, L., Hages, C. J., Schlatmann, R., Rech, B., Malinauskas, T., Unold, T., Kaufmann, C. A., Korte, L., Niaura, G., Getautis, V., Albrecht, S., Conformal monolayer contacts with lossless interfaces for perovskite single junction and monolithic tandem solar cells, *Energy Environ. Sci.* **12**, 3356-3369 (2019).
DOI: 10.1039/C9EE02268F

[46] Al-Ashouri, A., Köhnen, E., Li, B., Magomedov, A., Hempel, H., Caprioglio, P., Márquez, J. A., Morales Vilches, A. B., Kasparavicius, E., Smith, J. A. Phung, N., Menzel, D., Grischek, M., Kegelmann, L., Skroblin, D., Gollwitzer, C., Malinauskas, T., Jošt, M., Matič, G., Rech, B., Schlatmann, R., Topič, M., Korte, L., Abate, A., Stannowski, B., Neher, D., Stolterfoht, M., Unold, T., Getautis, V., Albrecht, S., Monolithic perovskite/silicon tandem solar cell with >29% efficiency by enhanced hole extraction, *Science* **370**, 1300-1309 (2020).
DOI: 10.1126/science.abd4016

[47] Kim, T. H., Lee, J. H., Jang, M. H., Lee, G. M., Shim, E. S., Oh, S., Saeed, M. A., Lee, M. J., Yu, B., Hwang, D. K., Park, C. W., Lee, S. Y., Jo, J. W., Shim, J. W., Atto-Scale Noise Near-Infrared Organic Photodetectors Enabled by Controlling Interfacial Energetic Offset through Enhanced Anchoring Ability, Adv. Mater. 2403647 (2024).
DOI: 10.1002/adma.202403647

[48] Liu, M., Li, M., Li, Y., An, Y., Yao, Z., Fan, B., Qi, F., Liu, K., Yip, H., Lin, F. R., Jen, A. K.-Y., Defect-Passivating and Stable Benzothiophene-Based Self-Assembled Monolayer for High-Performance Inverted Perovskite Solar Cells, Adv. Energy Mater. 14, 2303742 (2024).
DOI: 10.1002/aenm.202303742

[49] Zhang, H., Zhang, S., Ji, X., He, J., Guo, H., Wang, S., Wu, W., Zhu, W. H., Wu, Y., Formamidinium Lead Iodide-Based Inverted Perovskite Solar Cells with Efficiency over 25 % Enabled by An Amphiphilic Molecular Hole-Transporter, *Angew. Chem. Int. Ed.* **63**, e202401260 (2024).
DOI: 10.1002/anie.202401260

[50] Sze, S. M., Li, Y., Ng, Kwok K., *Physics of Semiconductor Devices*, 4th Ed., Wiley, New York, 2021, pp. 45-46.

[51] Mirzehmet, A., Ohtsuka, T., Abd. Rahman, S. A., Yuyama, T., Krüger, P., Yoshida, H., Surface Termination of Solution-Processed $CH_3NH_3PbI_3$ Perovskite Film Examined using Electron Spectroscopies, *Adv. Mater.* **33**, 2004981 (2020).
DOI: 10.1002/adma.202004981

[52] Endres, J., Egger, D. A., Kulbak, M., Kerner, R. A., Zhao, L., Silver, S. H., Hodes, G., Rand, B. P., Cahen, D., Kronik, L., Kahn, A., Valence and Conduction Band Densities of States of Metal Halide Perovskites: A Combined Experimental–Theoretical Study, *J. Phys. Chem. Lett.* **7**, 2722–2729 (2016).
DOI: 10.1021/acs.jpclett.6b00946

[53] Zu, F., Amsalem, P., Egger, D. A. Wang, R., Wolff, C. M., Fang, H., Loi, M. A., Neher, D., Kronik, L., Duhm, S., Koch, N., Constructing the Electronic Structure of $CH_3NH_3PbI_3$ and $CH_3NH_3PbBr_3$ Perovskite Thin Films from Single-Crystal Band Structure Measurements, *J. Phys. Chem. Lett.* **10**, 601-609 (2019).
DOI: 10.1021/acs.jpclett.8b03728

[54] Bi, H., Liu, J., Zhang, Z., Wang, L., Beresneviciute, R., Tavgeniene, D., Kapil, G., Ding, C., Baranwal, A. K., Sahamir, S. R., Sanehira, Y., Segawa, Hi., Grigalevicius, S., Shen, Q., Hayase, S., All-Perovskite Tandem Solar Cells Approach 26.5% Efficiency by Employing Wide Bandgap Lead Perovskite Solar Cells with New Monomolecular Hole Transport Layer, *ACS Energy Lett.* **8**, 3852-3859 (2023).
DOI: 10.1021/acsami.3c08655

[55] Bi, H., Liu, J., Beresneviciute, R., Tavgeniene, D., Zhang, Z., Wang, L., Kapil, G., Ding, C., Sahamir, S. R., Sanehira, Y., Baranwal, A. K., Kitamura, T., Wang, D., Wei, Y., Yang, Y., Kang, D. W., Grigalevicius, S., Shen, Q., Hayase, S., Efficiency Enhancement of Wide Bandgap Lead Perovskite Solar Cells with PTAA Surface-Passivated with Monomolecular Layer from the Viewpoint of PTAA Band Bending, *ACS Appl. Mater. Interfaces* **15**, 41549-41559 (2023).
DOI: 10.1021/acsami.3c08655

[56] Sze, S. M., Li, Y., Ng, Kwok K., *Physics of Semiconductor Devices*, 4th Ed., Wiley, New York, 2021, pp. 811-821.